Negative avalanche feedback detectors for photon-counting optical communications

William H. Farr

Jet Propulsion Laboratory, California Institute of Technology
4800 Oak Grove Drive, Pasadena, CA, USA 91109-8099

ABSTRACT

Negative Avalanche Feedback photon counting detectors with near-infrared spectral sensitivity offer an alternative to conventional Geiger mode avalanche photodiode or phototube detectors for free space communications links at 1 and 1.55 microns. These devices demonstrate linear mode photon counting without requiring any external reset circuitry and may even be operated at room temperature. We have now characterized the detection efficiency, dark count rate, after-pulsing, and single photon jitter for three variants of this new detector class, as well as operated these uniquely simple to use devices in actual photon starved free space optical communications links.

Keywords: single photon detector, photon counting, laser communications, optical communications, avalanche photodiode.

1. INTRODUCTION

Optical detectors with single photon sensitivity can achieve the highest bits per photon efficiency in an optical communications link [1]. An ideal single photon detector (SPD) would generate a readily distinguishable electrical output pulse for every incident photon, introduce zero timing jitter between photon arrival and electrical output, and have no false (dark or afterpulsing) counts. Furthermore, an ideal SPD would be low cost, available with any desired active area, and operate with no special environmental requirements.

Despite decades of development efforts, present SPD technologies are far from ideal, especially at the near-infrared (NIR) wavelengths near 1064 nm and 1550 nm important for optical communications. Examples of SPD technologies with sensitivity in the NIR spectral region include photomultiplier tubes (PMT) [2], intensified photodiodes (IPD) [3], superconducting nanowire SPDs (SNSPD) [4,5], and InGaAs semiconductor avalanche photodiodes (APD) [6].

Both the PMT and IPD devices utilize vacuum photoconductors with photocathode lifetimes on the order of ten thousand hours, are bulky, and require kilovolt bias supplies and cooling to -60 C or lower, although they do offer multi-mm^2 active detection areas. The SNSPD has exhibited high single photon detection efficiency (SPDE) at 1064 nm and 1550 nm, greater than 60% [7], but device areas are small, on the order of 10 - 100 μm^2, and this technology requires cryogenic cooling to 4.2 K or lower. InGaAs semiconductor APDs operated in Geiger mode (GM), whereby the detector is biased above breakdown, then triggered into continuous avalanche by either absorption of an incident photon or an internal "dark" event, followed by a reset of the avalanche by an external electrical circuit [8], are presently the most common NIR sensitive SPD. However, because of the high rate of dark carrier generation in InGaAs, and because of afterpulsing caused by the thermal release of trapped avalanche carriers after the initial photon detection pulse, device areas are typically limited to less than 1000 μm^2 and a minimum recovery (dead) time on the order of 1 μs is required between photon detections. Device cooling reduces the dark carrier generation rate, but increases the lifetime of trapped carriers, which increases the dead time before the detector can be re-biased above breakdown. For example, an InGaAs GM-APD with a 20 micron diameter might typically have a 300 KHz dark (false) count rate at 200K with a 10 μs dead time, resulting in a maximum count rate of less than 100 KHz [9].

1.1 SPD requirements for optical communications

Here we consider the case of a free space optical link for a photon starved channel, as encountered in an interplanetary laser communications scenario, for instance. We desire to minimize the required transmit energy per communicated bit, and to minimize the complexity and power requirements at the spacecraft transmitter, perhaps located in orbit at Mars or Jupiter. Furthermore, we shall assume a ground based receiver with the largest practical receiver aperture on Earth, and

Copyright 2009 California Institute of Technology. Government sponsorship acknowledged.

operation under both daytime and nighttime conditions. A simplified schematic for such a link using direct detection photon counting is depicted in Figure 1. The laser transmitter uses a high peak to average power pulse position modulation (PPM) [10] scheme to achieve a low gap to capacity [11]. The receive beam will be distorted by the Earth's atmosphere and the spot size on the detector will be at least D/r_0 times the wavelength diffraction limit, where D is the effective receive aperture diameter, and r_0 is the atmospheric coherence length. Thus a minimum detector area on the order of $2\pi(\lambda D/r_0)^2$ would be required, unless adaptive optics was utilized, but that would add considerable system complexity and be problematic for daytime operations. By combining photon counts digitally after detection (the discriminator in Figure 1), a large effective detector area can be achieved by pixilation, even across multiple receive apertures, if desired for performance, cost, or scaling reasons. After the discriminator, a receiver performs clock recovery, and a decoder recovers the encoded data [12].

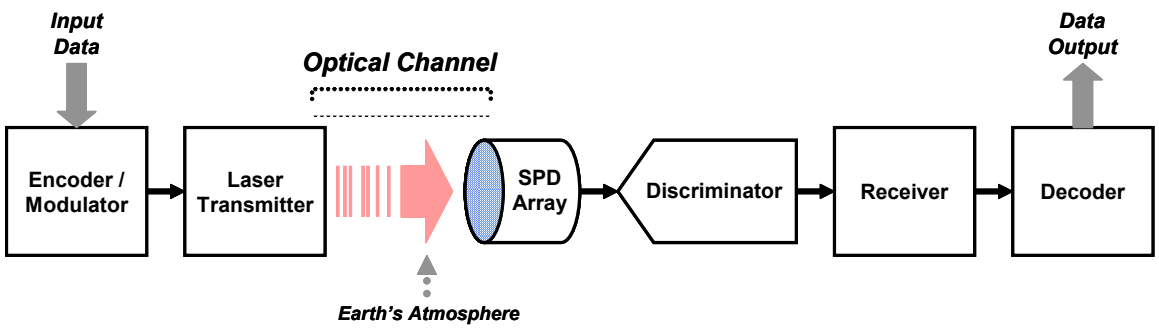

Fig. 1. Simplified block schematic for a photon counting direct detection optical communications link.

The ideal performing SPD detector would generate a distinguishable electrical pulse for every incident photon at the transmitter wavelength and generate no false pulse outputs. As the photon arrival time is critical for data recovery [13], the SPD should introduce no additional timing uncertainty over the $\Delta E \Delta t$ photon energy limit. Detector performance parameters characterize deviations from ideal, as summarized in Table 1.

Table 1. Primary SPD characterization parameters..

Parameter		Description	Typ. Units
Quantum Efficiency	QE	Ratio of generated primary photocarrier rate to incident photon rate	% (*unitless*)
Single Photon Detector Jitter	SPDE	Ratio of rate of distinguishable electrical output pulses to incident photon rate	% (*unitless*)
Dark Count Rate	DCR	Rate of distinguishable electrical output pulses (at a given SPDE operating point) with no optical input	Hz
After-Pulsing Ratio	APR	Ratio of correlated secondary distinguishable electrical output pulses to primary distinguishable electrical output pulses (at a given SPDE operating point)	% (*unitless*)
Single Photon Detection Jitter	SPDJ	Random timing jitter (uncertainty) between arrival time of incident photons to distinguishable electrical output pulses	s
Recovery Time		Time after a photon detection event for the SPDE to recover to a specified fraction of the limiting (maximum) SPDE value	s
Saturation Rate		Mean rate of distinguishable electrical output pulses under continuous wave (Poission) illumination for which apparent SPDE drops to a specified fraction of its limiting (low rate, maximum) value	Hz

Copyright 2009 California Institute of Technology. Government sponsorship acknowledged.

Many parameters in Table 1 refer to "distinguishable electrical output pulses." This indicates that the observed performance is not just a function of the SPD, but is also a function of the characterization system, typically a pulse discriminator followed by some form of counter. Additional detector parameters not mentioned in Table 1 include items such as detector mean gain and gain variance, and pulse bandwidth parameters such as rise and fall times. These parameters, in conjunction with characterization system noise and bandwidth performance, establish the criteria for a distinguishable electrical output pulse.

1.2 Semiconductor APD operational modes

Figure 2 shows a typical reverse bias I-V plot for a semiconductor APD with a separate absorption and multiplication structure, as is common for a III-V material system device such as an InGaAs/InP APD. Curves for non-illuminated and multiple illuminated conditions are depicted. Various operational modes correspond to different bias regions. In region **A**, the internal electric field is too weak to pull photocarriers into the multiplication region, and only a small leakage current is present for both the illuminated and dark conditions. In region **B**, sufficient field exists to pull photocarriers out of the absorption region before they recombine, but field bias in the multiplication region is insufficient to create avalanche gain. In region **B**, the SPD performs similar to a common PIN device structure. Avalanche gain begins to occur in region **C**, with the gain exponentially increasing in region **D** just below breakdown. Regions **B** and **C** constitute the linear operational mode of the APD, and in that region the difference between the illuminated and dark conditions is readily apparent. Region **E** constitutes device breakdown, whereby device current must be limited by an external circuit, otherwise the device will be destroyed. For GM operation, the APD is biased into region **E**, but breakdown does not occur until either an internal dark or external photon absorption event triggers the avalanche.

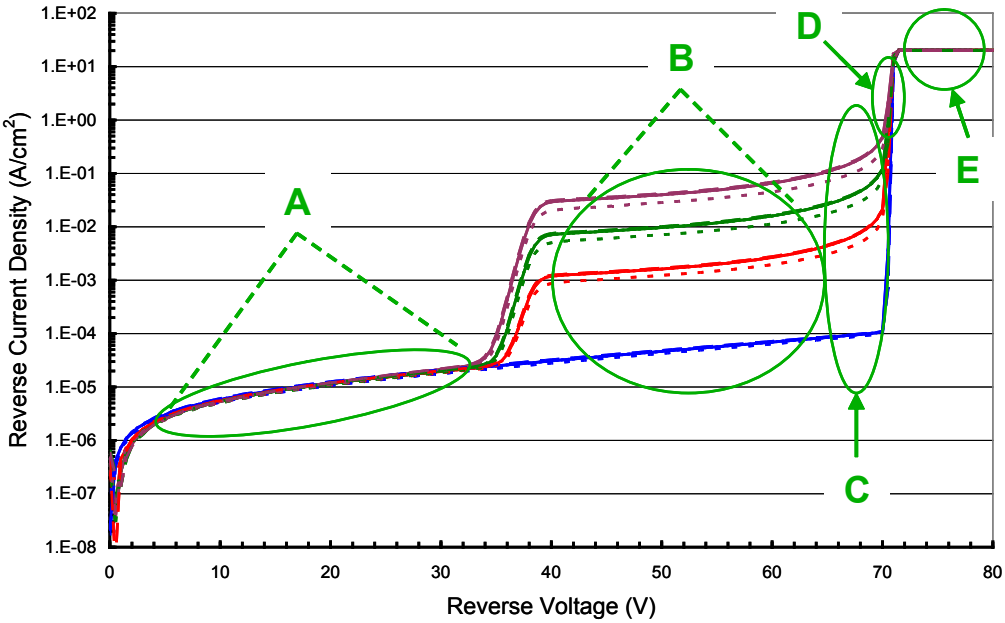

Fig. 2. APD bias regimes. **A** is below reach-through. **B** is unitary gain linear mode. **C** is linear avalanche gain (1 to 1000) mode. **D** is high avalanche gain (1000 to 10^5) sub-Geiger mode. **E** is breakdown (current limited by external circuit).

The gain in region **C** is insufficient to generate a readily distinguishable electrical output pulse corresponding to a single photon absorption event due to thermal noise in external electronics, even for cryogenically cooled amplifiers, and photon counting operation is not achieved. Single photon absorption events are readily detectable in the GM region **E**, but as noted above, the avalanche must be externally reset. Photon counting is possible in region **D** [14], sometimes referred to as sub-Geiger mode, but operation in that mode is unstable, as the device gain has very strong voltage bias and temperature dependence [15], whereby milliVolt bias and sub-degree temperature drifts can either drop device gain

Copyright 2009 California Institute of Technology. Government sponsorship acknowledged.

below 1000 or drive the detector into breakdown. Another factor limiting photon counting performance is gain variance, F, in the avalanche process, $F = \langle M^2 \rangle / \langle M \rangle^2$, where M is the avalanche gain for a single photon absorption event. The common model for this gain variance is described by Webb-McIntyre-Conradi statistics [16], which is a function of both the mean gain $\langle M \rangle$ and an idealized coefficient k related to the electron-hole mobility ratio in the multiplication region. Note that even for $k=0$, gain variance under the classic semiconductor avalanche process is too high to allow single versus two photon absorption events to be reliably discriminated. These results are summarized in Table 2.

Table 2. APD response to single photon absorptions by operational mode.

Mode	Mean Gain $\langle M \rangle$	Gain Distribution	Excess Noise Model $F = \frac{\langle M^2 \rangle}{\langle M \rangle^2}$	Recovery Time	Single Photon Pulse Response
Linear	1 - 1000	Gamma	$F = k\langle M \rangle + (1-k)\left(2 - \frac{1}{\langle M \rangle}\right)$ McIntyre/Conradi Statistics	None	
Sub-Geiger	1000 - 1.E6	Exponential		Equal to electrical pulse width	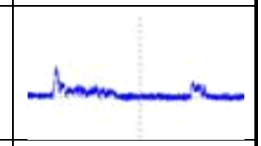
Geiger	> 1.E6	Unbounded	"Infinite" excess noise	External reset, followed by "dead" time, 10 – 1000 ns	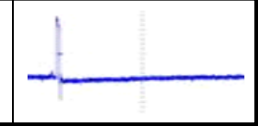

2. NEGATIVE AVALANCHE FEEDBACK SEMICONDUCTOR APD'S

By the time an external reset circuit detects the presence of an output pulse from an InGaAs GM-APD and quenches the avalanche, on the order of 10^6 carriers have passed through the gain region. This is excessive, as a nanosecond width output pulse with only 10^4 carriers can easily be amplified by a low cost SiGe broadband RF amplifier to milliVolt levels, which can be easily read by digital processing circuitry. By reducing the avalanche charge, the probability of an afterpulse can be minimized, and the APD can be (a) operated at a lower temperature to reduce the dark count rate (DCR) and (b) operated with a reduced recovery time to enable higher count rates and a broader dynamic range. Gains of 10^4 to 10^5 can be achieved by biasing the APD into the sub-Geiger region **D** of Figure 2, but in addition to the instability noted above, the exponential gain distribution noted in Table 1 implies that most photon absorptions result in much smaller gains than $\langle M \rangle$, such that most output pulses are not above the electronics thermal noise floor. Thus the SPDE in sub-Geiger mode is much lower than that obtainable in full Geiger mode.

To circumvent the drawbacks of sub-Geiger mode, JPL has worked with several industrial and academic partners to develop a new class of semiconductor SPD with NIR sensitivity. The key feature has been to modify the detector device structure to introduce Negative Avalanche Feedback (NAF) into the multiplication region. The NAF mechanism reduces the variance of the gain. The NAF mechanism also greatly reduces fluctuations in mean gain due voltage bias and operating temperature drifts, essentially turning the multiplication region into a limiting amplifier. A further benefit is that the device is self-resetting with effective recovery times on the order of tens of nanoseconds or less.

The first device to effectively demonstrate a NAF mechanism in a III-V material system APD was the transient carrier buffer (TCB) structure developed at the University of California at San Diego (UCSD) [17,18]. Subsequently, alternate device structures to implement the NAF mechanism have been developed by Princeton Lightwave, Inc. (PLI), and most recently by Amplification Technology, Inc. (ATI). PLI refers to its technology as a negative feedback avalanche diode (NFAD), while ATI calls its technology a discrete amplification photon detector (DAPD). All three technologies use an InGaAs absorber for 0.9 to 1.6 micron sensitivity, but differ in their implementations of the avalanche gain structure.

One feature of the InGaAs NAF detectors is that they can be implemented with larger device areas than possible with a conventional InGaAs GM-APD. The NAF structure can simultaneously limit both the charge variance and the spatial

Copyright 2009 California Institute of Technology. Government sponsorship acknowledged.

extent of an avalanche pulse, with the result that larger device areas are capable of photon number resolution in nanosecond or shorter optical pulses.

Both, either, or neither the absorption and multiplication regions can be pixilated when implementing larger device areas. The UCSD device uses monolithic absorber and gain regions for larger areas. The PLI device is pixilated at the absorber and gain level. The ATI device uses a monolithic absorber and a pixilated gain region. The limit on device area is a function of output pulse width and dark count rate. The largest devices tested to date that demonstrate single photon response are ATI DAPDs with a 210 μm diameter (34618 μm^2) operating at 265K. All of the devices can be implemented as multiple output arrays to achieve spatial resolution and to increase performance under high illumination.

The InGaAs NAF detectors are DC biased, free running, self resetting, NIR sensitive SPDs that can even operate at room temperature, although cooling in the 270K down to 180K range is desirable to reduce DCR.

3. NAF DETECTOR CHARACTERIZATION

To understand the potential optical link performance of the InGaAs NAF technologies, and to better understand their performance limitations in order to guide future device development, devices have been characterized at both 1064 nm and near 1550 nm under both continuous wave (CW) and short pulse (5 ps) illumination. Note that all devices tested are early generation devices, and performance improvements are expected.

3.1 Temporal pulse characteristics

Figure 3 shows sample single photon response pulses from ATI and PLI NAF detectors. The DAPD devices (3a) have the fastest response to date with a full width half maximum (FWHM) of 700 ps (independent of device area), as compared to the NFAD device (3b) FWHM of around 1.5 ns. Early TCB devices had FWHMs around 30 ns, but newer devices have pulse widths less than two nanoseconds.

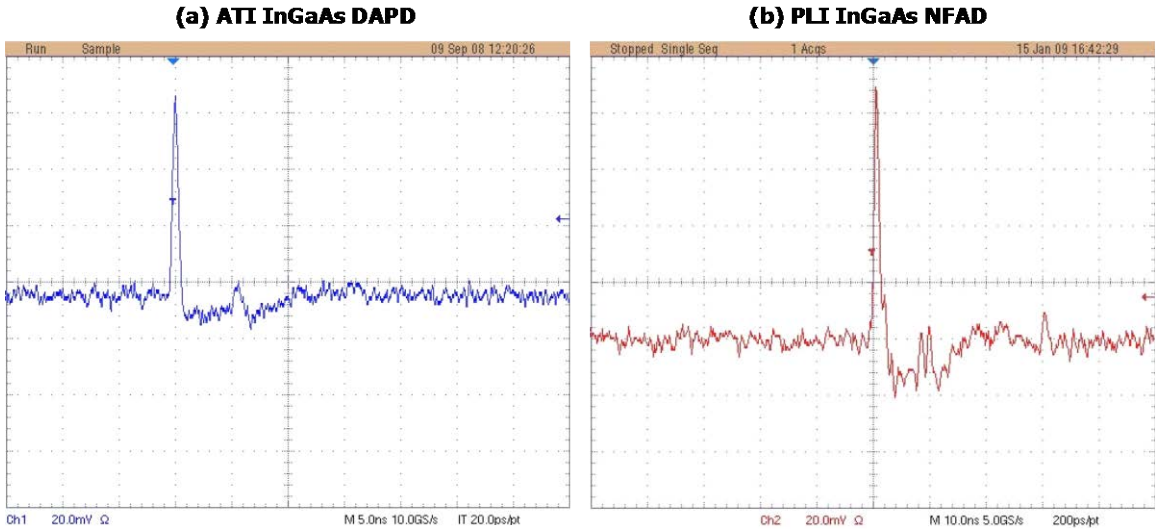

Fig. 3. (a) Single photon response from ATI 94 μm diameter DPAD at 293K and 53.1 V reverse bias. (b) Single photon response from PLI 16 μm diameter NFAD device at 242K and 76.0 V reverse bias.

As seen in the inset in Figure 4, NAF devices are free-running with no pre-determined hold-off time between pulses. The corresponding amplitude histogram is computed from a ¼ second sequence of that data using a hysteresis filter to determine peak pulse amplitude. The hysteresis filter defines a peak as any positive going peak that then drops more than 2% of digitizer full scale. The single photon response peaks are well resolved from the thermal noise floor, which is responsible for the off-scale central peak in Figure 4.

Copyright 2009 California Institute of Technology. Government sponsorship acknowledged.

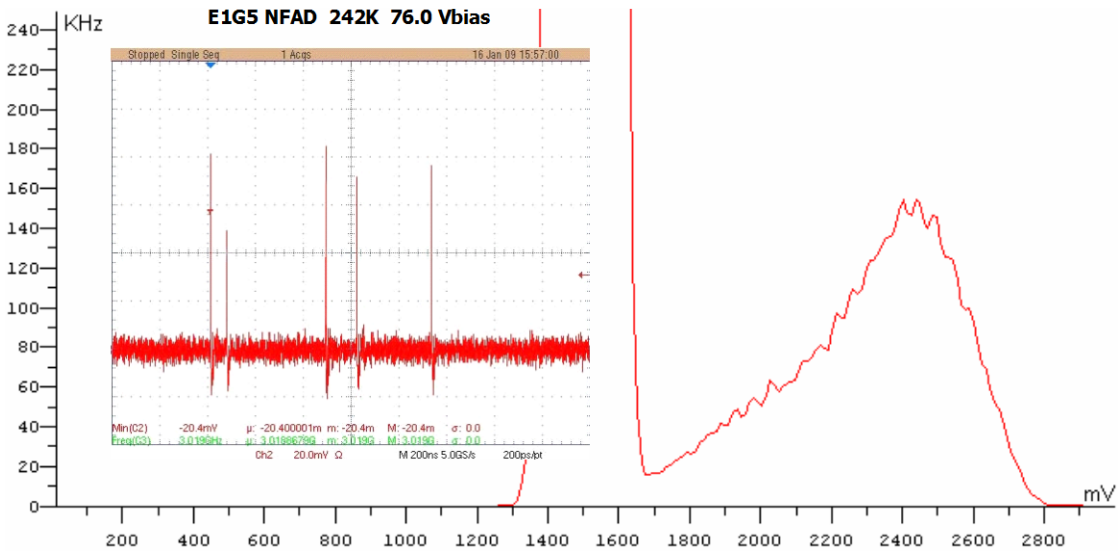

Fig. 4. Pulse amplitude histogram from PLI 16 µm diameter NFAD device at 242K and 76.0 V reverse bias. The area above a 1700 mV threshold corresponds to a count rate of 6.9 MHz under frontside illumination. DCR was 24.5 KHz.

3.2 Gain and gain variance characterization

Pulse amplitude histograms, as in Figure 4, are insufficient to determine device gain and excess noise. A pulse charge histogram is formed by integrating the current flowing into the device load (50 Ohms typically) for each pulse. Figure 5 shows an example pulse charge histogram for a UCSD TCB detector, along with an inset showing mean gain and excess noise factor as a function of reverse bias voltage.

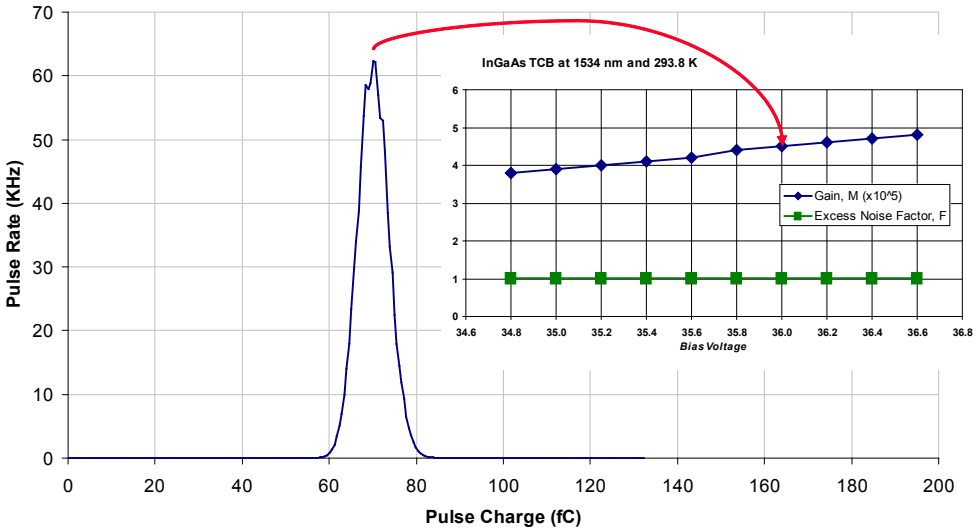

Fig. 5. Example UCSD TCB pulse charge histogram used to compute device gain and excess noise factor as a function of bias voltage (as shown in the inset). Gain distribution shown is for 36.0 V bias

The excess noise for this device is less than 1.01 and the gain remains near 4.5×10^5 even over a two Volt reverse bias range, a clear indication of a functional NAF mechanism.

Copyright 2009 California Institute of Technology. Government sponsorship acknowledged.

3.3 Single photon jitter characterization

SPDJ has been characterized for the NAF devices using a 1550 nm mode-locked laser source with 5 ps pulse widths and a single channel analyzer (SCA) technique. The SCA histogram is triggered by the mode-locked laser pulse and records the arrival time of the first electrical pulse above threshold out of the detector. Figure 6 shows typical SCA histograms for present generation DAPD and NFAD devices.

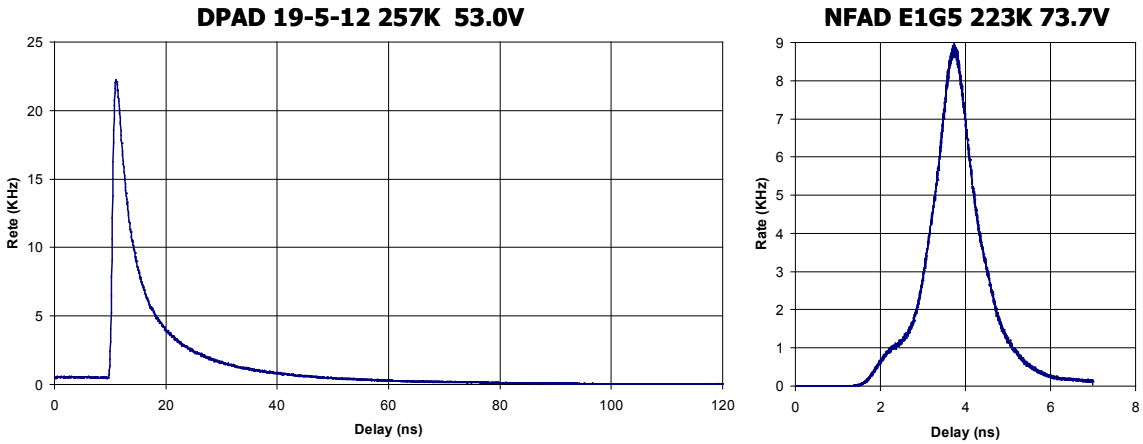

Fig. 6. SCA timing histograms for SPDJ measurement.

The optical communications performance loss due to SPDJ is best represented as a one sigma (1σ) value, as opposed to the commonly used timing peak FWHM [13]. This is because events outside the main timing peak cannot be excluded from the receiver signal chain. The 1σ SPDJ for the NFAD detector is 240 ps. The slight bump on the front side of the timing peak has been observed to increase with further device cooling, and may be an artifact of the frontside illumination used to characterize the device in the present test fixture, whereas the devices are designed for backside illumination.

The 1σ for the DAPD device is much longer, 13.5 ns. A probable cause for this excessive jitter is that the first generation DAPD devices were designed to have poor coupling between the absorber and multiplication layers to minimize the chance that the NAF mechanism would be overwhelmed by large dark current from the absorber layer. The poor coupling is evident upon cooling the devices below about 260K, whereupon the SPDE begins to drop as the maximum allowable bias voltage before full breakdown decreases with cooling, and at this point the internal field is insufficient to pull carriers from the absorber layer into the multiplication region.

SPDJ for the TCB detector has been measured to be 850 ps at 280K.

3.4 Recovery time characterization

Recovery time can be characterized from pulse interarrival time histograms under CW illumination. For an optical source with Poisson statistics, the interarrival times should follow an exponential distribution. A semi-log plot of the pulse interarrival times should show a linear slope. Response below the linear slope represents decreased effective SPDE for that inter-pulse interval. Response above the linear slow represents after-pulsing effects that give a false high SPDE. Such a plot for an NFAD device is shown in Figure 7. The recovery and after-pulsing regions are clearly visible in this figure with a recovery time for the NFAD device of about 20 ns.

The DAPD device structure is such that it effectively has no recovery time. More properly, the recovery time for the DAPD is on the order of its 10% pulse height pulse width, about one nanosecond.

Recovery times for TCB devices are strongly bias and temperature dependant and in the 60 ns to 100 ns range.

Copyright 2009 California Institute of Technology. Government sponsorship acknowledged.

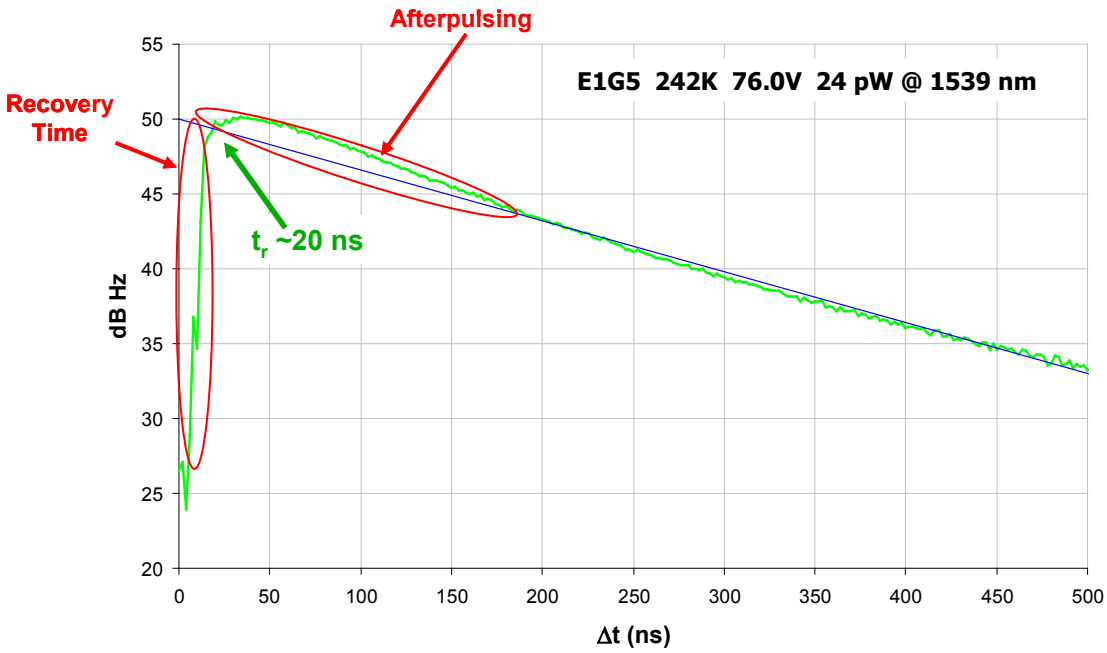

Fig. 7. Interarrival time histogram for recovery time measurement, also showing the presence of after-pulsing for the NFAD device. Device is illuminated with a filtered thermal source or attenuated CW laser beam for this measurement.

3.5 After-pulsing characterization

Although APR can be determined from an interarrival time histogram, we prefer a more direct method using a 1550 nm mode-locked laser source with 5 ps pulse widths and a multi-channel analyzer (MCA). The MCA histogram is triggered by the mode-locked laser pulses and records the arrival time of the every electrical pulse above threshold out of the detector relative to that trigger event. Figure 8 shows an MCA histogram for an NFAD device using one nanosecond timing bins and a 731 KHz pulse repetition frequency.

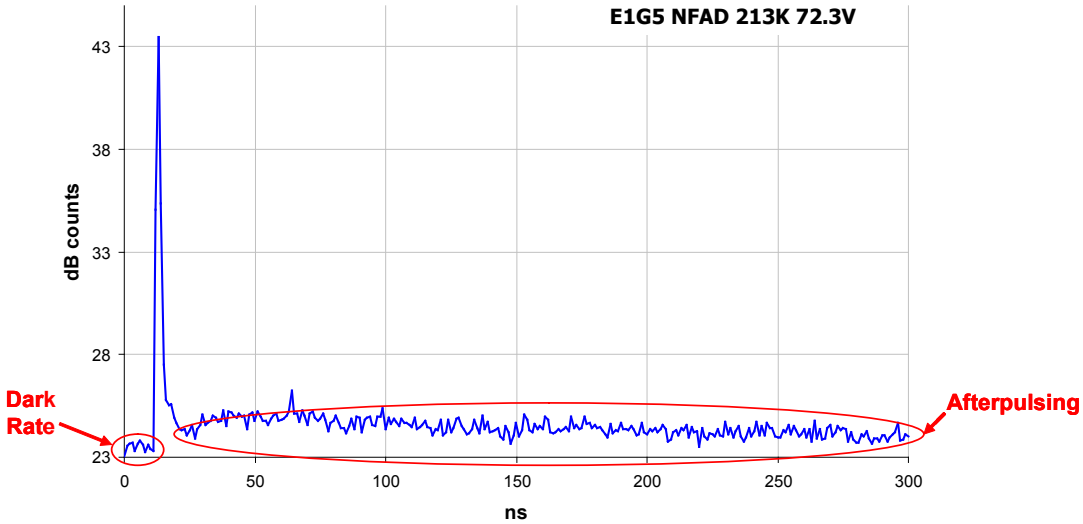

Fig. 8. MCA histogram for recovery time measurement for an NFAD device. The pedestal before the main timing peak represents the device dark rate. The elevated pedestal after the main timing peak contains both dark and after- pulses.

Copyright 2009 California Institute of Technology. Government sponsorship acknowledged.

The after-pulsing pedestal in Figure 8 represents a 30% APR for the NFAD device. The APR for the DAPD is even worse, around 50%, and the APR for the TCB detector has not yet been quantified.

Clearly, after-pulsing is a dominant problem. We hope to achieve APR levels less than 1% by optimization of operating conditions, reduction of device gain, and better materials processing to reduce the number of trap sites in the multiplication and negative feedback layers.

3.6 Saturation, SPDE and DCR

Although SPDE and DCR can be determined from calibrated optical sources and pulse histograms, such as depicted in Figure 4, these measurements will overestimate SPDE due to after-pulsing, and underestimate SPDE at high incident flux rates due to saturation. Saturation affect are depicted in Figure 9 for a 94 μm diameter DAPD.

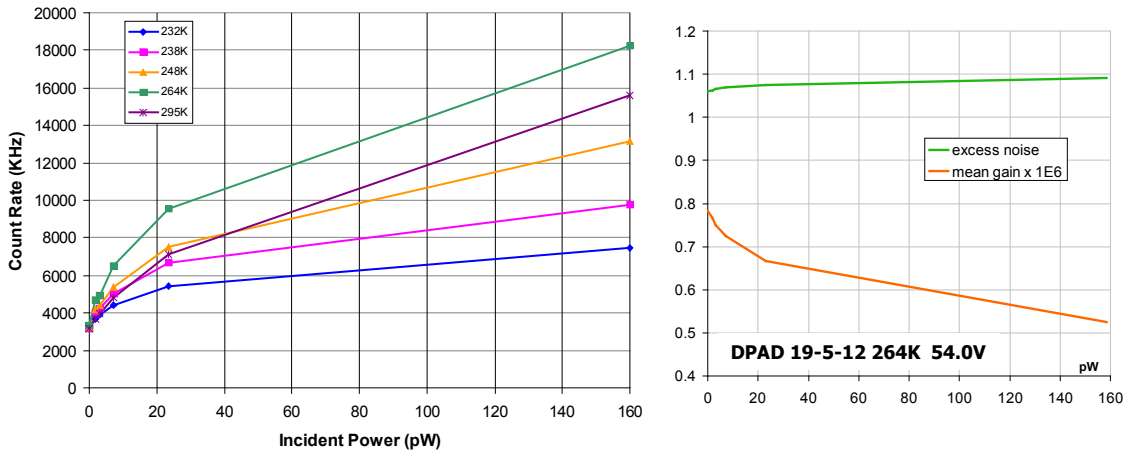

Fig. 9. (a) Left plot show variations in achievable count rate and high illumination saturation for a 94 mm diameter DPAD. (b) Right plot shows gain and excess noise factor variation corresponding to the 264 K curve.

The SPDE loss in NAF detectors can generally be attributed to a decrease in mean gain and increase in gain variance. Unlike GM-APDs, the NAF SPD performance degrades to that of a conventional linear APD under bright illumination.

SPDE and DCR can be directly extracted from MCA histograms, as depicted in Figure 8. For accurate measurements the laser pulse is attenuated to a mean number of photons per pulse of 0.05 or less to minimize the probability of a multi-photon pulse to less than 0.13%.

Table 3 summarizes present performance parameters for InGaAs TCB, NFAD, and DAPD NAF SPDs. The performance demonstrated by these early generation prototype detectors should be considered "proof of concept," and much progress can be expected over the next few years.

Table 3. Prototype NAF detector performance summary

	TCB	NFAD	DAPD	Note
SPDE	14%	6%	8.5%	highest measured to date
DCR	6 MHz	0.1 MHz	3 MHz	at highest SPDE
APR	not measured	30%	50%	at highest SPDE
SPDJ	850 ps	240 ps	13.5 ns	1-σ at highest SPDE
recovery	60 ns	20 ns	1 ns	at highest SPDE
saturation	3 MHz	8 MHz	5 MHz	1 dB loss; function of detector area

Copyright 2009 California Institute of Technology. Government sponsorship acknowledged.

4. OPTICAL LINK PERFORMANCE

Although the NAF SPDs are at an early stage of development, and the NFAD and DAPD devices have exhibited excessive after-pulsing, in Figure 10 we illustrate the measured performance of a DAPD detector in an end-to-end optical communications test bed. The test bed utilized a rate 1/2 error-correction-code, M=16 PPM, and performs slot and symbol synchronization utilizing an embedded guard-time slot [19]. The noise background was at 0.0127 mean detected noise photons/slot. The NAF detector achieved a photon efficiency of 1.59 bits/detected photon.

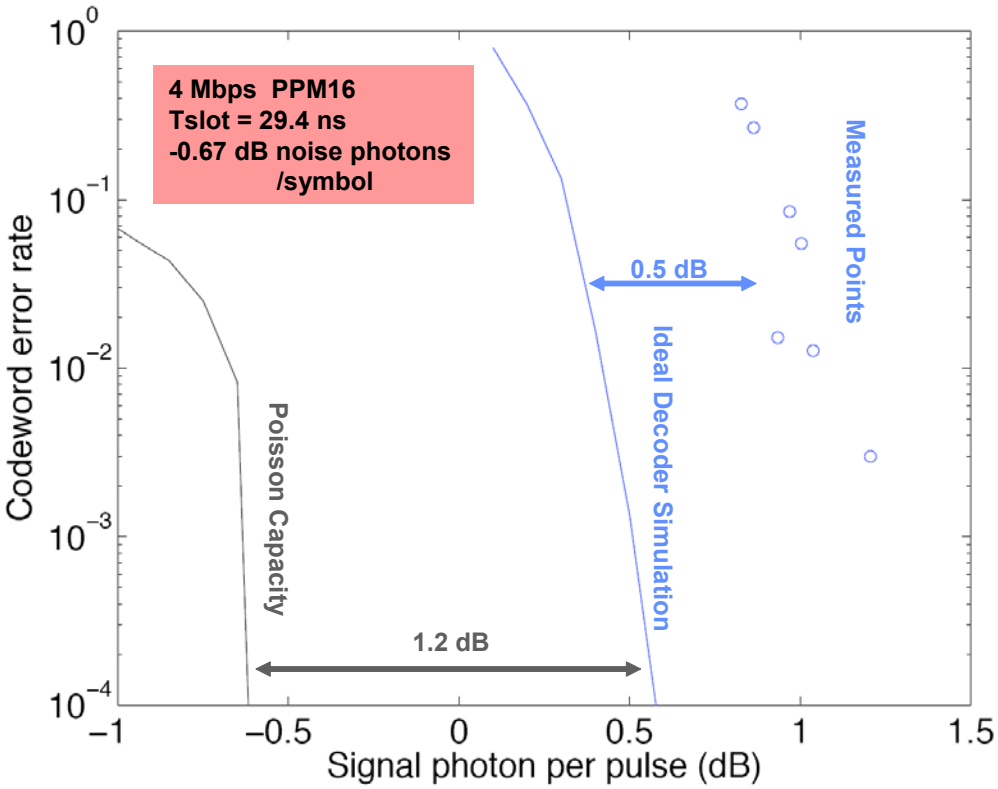

Fig. 10. Free space photon counting link using a DAPD device at 1064 nm. Rates are detected mean photon rates. Observed loss relative to the ideal receiver/decoder may be attributed to jitter and finite quantization in the hardware.

5. CONCLUSIONS

NAF technology SPDs are an exciting new approach to photon counting detectors. NAF detectors are simple two terminal semiconductor SPDs requiring only a DC bias and low cost RF amplifier to amplify single photon electrical output pulses to levels suitable for input to digital processing circuitry. NAF detectors are free-running and self-resetting. The devices can photon count at room temperature, and simple thermoelectric cooling can greatly reduce DCR. As much of the NAF device structure is similar to a conventional GM-APD structure, we expect that future device generations will achieve similar SPDE, DCR, APR, and SPDJ. Removal of the requirement for per-pixel reset circuitry can greatly simplify photon counting optical communications system implementations. NAF devices have already been fabricated as small arrays to 8x8 pixels, and larger format arrays (32x32 to 128x128), are possible.

Acknowledgements: The author gratefully acknowledges Kai Zhao, Authur Zhang, and Yu-Hwa Lo of UCSD for supplying TCB detectors, Mark Itzler and Xudong Jiang of PLI for supplying NFAD detectors, and Alex Krutov and Krishna Linga of ATI for supplying DAPD detectors. The author would like to thank Bruce Moision for the photon counting link simulation. The work described here was performed at the Jet Propulsion Laboratory (JPL), California Institute of Technology under contract with the National Aeronautics and Space Administration (NASA).

Copyright 2009 California Institute of Technology. Government sponsorship acknowledged.

REFERENCES

[1] Y. Yamamoto, H. A. Haus, "Preparation, measurement, and information capacity of optical quantum states," Rev. Mod. Phys., vol. 58, pp. 1001-1020, 1986

[2] A. Biswas, W. H. Farr, "Laboratory Characterization and Modeling of a Near-Infrared Enhanced Photomultiplier Tube," IPN Progress Report 42-152, 2003

[3] Ross A. La Rue, Kenneth A. Costello, Gary A. Davis, John P. Edgecumbe and Verle W. Aebi, "Photon Counting III-V Hybrid Photomultipliers Using Transmission Mode Photocathodes", IEEE Transactions on Electron Devices, vol. 44, no. 4, April 1997

[4] G. Gol'tsman, et al., "Picosecond superconducting single-photon optical detectors," Appl. Phys. Lett., vol. 79, pp. 705-707, 2001

[5] J. A. Stern and W. H. Farr, "Fabrication and Characterization of Superconducting NbN Nanowire Single Photon Detectors," IEEE Transactions on Applied Superconductivity, vol. 17, no. 2, Jun. 2007

[6] M. A. Itzler, R. Ben-Michael, C. F. Hsu, K. Slomkowski, A. Tosi, S. Cova, F. Zappa, R. Ispasoiu, "Single photon avalanche diodes for 1.5 μm photon counting applications," Journal of Modern Optics, vol. 54, nos. 2-3, pp. 283-304, Feb. 2007

[7] K. M. Rosfjord1, J. K.W. Yang1, E. A. Dauler, A. J. Kerman, V. Anant1, B. M. Voronov, G. N. Gol'tsman, K. K. Berggren, "Nanowire single-photon detetctor with an integrated optical cavity and anti-reflection coating," Opt. Express, pp. 527–534, 2006

[8] I. Prochazka, "Peltier-cooled and actively quenched operation of InGaAs/InP avalanche photodiodes as photon counters at a 1.55-μm wavelength," Applied optics, vol. 40, no. 33, pp. 6012-6018, Nov. 2001

[9] S. Pellegrini , R. E. Warburton , L. J. J. Tan , J. S. Ng , A. B. Krysa , K. Groom , J. P. R. David , M. J. Robertson and G. S. Buller, "Design and performance of an InGaAs-InP single-photon avalanche diode detector," IEEE J. Quantum Electron., vol. 42, pp. 397, Apr. 2006

[10] R. G. Lipes, "Pulse-position-modulation coding as near-optimum utilization of photon counting channel with bandwidth and power constraints, " DSN Progress Report, vol. 43, pp. 108-113, Apr. 1980

[11] B. Moision and J. Hamkins, "Coded modulation for the deep space optical channel: serially concatenated PPM," IPN Progress Report, vol. 42-161, 2005

[12] A. Biswas, et. al, "Palomar receive terminal for the Mars laser communication demonstration project", Proc. Of the IEEE, vol. 95, no. 10, pp. 2045-2058, 2007

[13] B. Moision and W. Farr, "Communication Limits Due to Photon Detector Jitter," IEEE Photonics Technology Letters, vol. 20, no. 9, May 2008

[14] T. Maruyama, F. Narusawa, M. Kudo, M. Tanaka, Y.i Saito, A. Nomura, "Development of a near-infrared photon-counting system using an InGaAs avalanche photodiode," *Optical Engineering*, vol. 41, no.2, Feb. 2002

[15] C. L. F. Ma, M. J. Deen, L. E. Tarof, J. C. H. Yu, "Temperature Dependence of Breakdown Voltages in Separate Absorption, Grading, Charge, and Multiplication InP/InGaAs Avalanche Photodiodes," IEEE Trans. On Electron Devices, vol. 42, no. 5, pp. 810-818, May 1995

[16] P. P. Webb, R. J. McIntyre, J. Conradi, "Properties of Avalanche Photodiodes," RCA Review, vol. 35, pp. 234-278, June 1974

[17] K. Zhao, A. Zhang, Y. Lo, W. Farr, "InGaAs single photon avalanche detector with ultralow excess noise", *Appl. Phys. Lett*. 91, 081107 (2007)

[18] K. Zhao, S. You, J. Cheng, Y. Lo, "Self-quenching and self-recovering InGaAs/InAlAs single photon avalanche detector", *Appl. Phys. Lett*.. 93, 153504 (2008)

[19] K. Birnbaum, W. Farr, J. Gin, B. Moision, K. Quirk, M. Wright, "Demonstration of a high-efficiency free-space optical communications link," Proc. SPIE, 7199, 7199-09 (2009)

Copyright 2009 California Institute of Technology. Government sponsorship acknowledged.